The Chinese University of Hong Kong, Shenzhen

PHY1002

Physics Laboratory

Driven Damped Harmonic Oscillations

Author:
Yohandi

Student Number:
120040025

April 17, 2023

Contents

1. Objective

1.1. Theory Review

1.1.1. Harmonic Oscillation

The oscillating system in this experiment consists of a disk connected to two springs. A string connecting the two springs is wrapped around the disk so the disk oscillates back and forth. This is like a torsion pendulum. The period of a torsion pendulum without damping is given by:

$$T = 2\pi\sqrt{\frac{I}{\kappa}} \tag{1}$$

where I is the rotational inertia of the disk and κ is the effective torsional spring constant of the springs. The rotational inertia of the disk is found by measuring the disk mass (M) and the disk radius (R). For a disk, oscillating about the perpendicular axis through its center, the rotational inertia is given by:

$$I = \frac{1}{2}MR^2 \tag{2}$$

The torsional spring constant is determined by applying a known torque ($\tau = rF$) to the disk and measuring the resulting angle (θ) through which the disk turns. Then the spring constant is given by:

$$\kappa = \frac{\tau}{\theta} \tag{3}$$

1.1.2. Damped Harmonic Oscillation

If a damped oscillator is displaced from equilibrium and allowed to oscillate and damp out, the equation of motion is

$$\frac{d^2\theta}{dt^2} + \frac{\mathtt{b}}{I}\frac{d\theta}{dt} + \frac{\kappa}{I}\theta = 0 \tag{4}$$

, where $\mathtt{b}$ is the damping coefficient, I is the rotational inertia, and κ is the spring constant. Then, to the equation above, the solution is given by:

$$\theta = \theta_0 e^{-\frac{b}{2I}t}\sin(\omega t + \phi) \tag{5}$$

, where the angular frequency is given by:

$$\omega = \sqrt{\frac{\kappa}{I} - \frac{b^2}{4I^2}} \tag{6}$$

1.1.3. Driven Damped Harmonic Oscillation

When the damped oscillator is driven with a sinusoidal torque, the differential equation describing its motion is

$$I\frac{d^2\theta}{dt^2} + \mathtt{b}\frac{d\theta}{dt} + \kappa\theta = \tau_0 \mathtt{cos}(\omega t) \tag{7}$$

The solution to this equation is

$$\theta = \frac{\frac{\tau_0}{I}}{\sqrt{(\omega^2 - \omega_0^2)^2 + \frac{\mathtt{b}}{I}^2\omega^2}}\mathtt{cos}(\omega t - \phi) \tag{8}$$

, where the amplitude of the oscillation is

$$\theta_0 = \frac{\frac{\tau_0}{I}}{\sqrt{(\omega^2 - \omega_0^2)^2 + \frac{\mathtt{b}}{I}^2\omega^2}} \tag{9}$$

and the phase difference between the driving torque is

$$\phi = \mathtt{tan}^{-1}(\frac{\frac{\omega \mathtt{b}}{I}}{\omega_0^2 - \omega^2}) \tag{10}$$

The resonant frequency ω_0 can be given as

$$\omega_0 = \sqrt{\frac{\kappa}{I}} \tag{11}$$

. When the driving frequency is equal to the resonant frequency, the amplitude is maximum. If we set $\omega = \omega_0$ to equation (9), we have

$$\theta_0 = \frac{\tau_0}{\mathtt{b}}\sqrt{\frac{I}{\kappa}} \tag{12}$$

1.2 Aim of Experiment

In this experiment, we aim to investigate the behavior of a driven damped harmonic oscillator, specifically consisting of an aluminum disk, a pulley, and two springs. The system exhibits oscillatory motion when subjected to both an opposing damping force and an external driving force, causing it to move periodically and harmonically around an equilibrium position. The objective is to understand how the amplitude of the oscillations varies with the driving force frequency and different levels of magnetic damping, as well as to evaluate the motion of the aluminum disk as it experiences driven damped harmonic oscillations.

Two Rotary Motion Sensors are employed to record the angular positions and velocities of the disk and the driver as a function of time. The system is modeled using the equation of motion for a simple harmonic oscillator, but with the addition of a driving force term to account for the external force applied to the system. The amplitude of the oscillation is plotted against the driving frequency, enabling the investigation of the system's response to different levels of energy input.

An adjustable magnet is utilized to provide varying amounts of magnetic damping, which can be controlled by moving it closer to or farther from the aluminum disk. This experimental setup allows for the exploration of the effects of damping on the system's

behavior, including resonant behavior, damping, and nonlinearity. Moreover, the dependence of the phase difference (φ) on different driving frequency values will be examined, specifically when equal to zero, at resonance, and as it approaches infinity.

2. Method

2.1. Setup

Figure 1: Driver

Figure 2: Complete Setup

Begin the experiment setup by mounting the driver on a rod base and setting the driver arm amplitude at about half maximum. Attach the first Rotary Motion Sensor to the

same rod, ensuring it is oriented as shown in Figure 2. Rotate the driver arm so it is vertically downward, then attach a string to it. Thread the string through the string guide and wrap it around the Rotary Motion Sensor's large pulley. Tie the end of the string to a spring, which should be connected close to the Rotary Motion Sensor.

To increase stability, use two vertical rods connected by a cross rod at the top, as depicted in Figure 2. Mount the second Rotary Motion Sensor on the cross rod. Proceed by tying a short string to the leveling screw on the base, and attach one end of the second spring to this string. Cut another string to approximately 125 cm, wrap it around the large pulley of the second Rotary Motion Sensor, and secure the disk to the Rotary Motion Sensor using a screw.

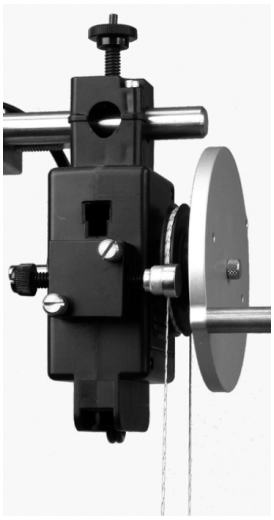

Figure 3: String and Magnet

Thread the ends of the string from the pulley through the springs and tie them off, ensuring equal tension on each side. The disk should be able to rotate 180 degrees without the springs touching the Rotary Motion Sensor pulley. Attach the magnetic drag accessory to the side of the Rotary Motion Sensor, positioning the magnet about 1.0 cm from the disk. The magnet generates damping force, which can be adjusted by altering the distance between the magnet and the disk.

Plug the disk Rotary Motion Sensor into Channel P1 and the driver Rotary Motion Sensor into Channel P2, setting the sample rate for both sensors to 50 Hz. Ensure the rotary motion sensors read positive in the same direction. In PASCO Capstone's Hardware Setup, configure Signal Generator 1 to a Negative Ramp with a frequency of 0.001 Hz, amplitude of 3.1 V, and a DC offset of 6.1 V, then set it to Off.

Connect the banana cords from the driver to Signal Generator 1 on the 850 Universal Interface. The voltages regulate the driver's rotation speed. The stop condition is set when the Output Voltage falls below 3.1 V. Follow the instructions provided, but be aware of the incorrect plug shown in Figure 2; instead, adhere to the written directions for plugging in the Rotary Motion Sensors.

2.2. Procedure

2.2.1. Resonant Frequency

To ascertain the resonant frequency of the system, begin by manually rotating the disk to a specific position and releasing it. Utilize the Rotary Motion Sensor to capture the disk's angular speed as a function of time, and then cease recording. Employ the coordinates tool within the PASCO software to measure the oscillation period by determining the time between two consecutive peaks or troughs on the angular speed versus time graph. During this process, ensure the magnet is removed; otherwise, the collected data will be rendered invalid.

2.2.2. Spring Constant

First, attach the golden cylinder mass to a spring and hold it in position. Before releasing the cylinder, initiate the recording to accurately capture the graph. Upon starting the recording, release the cylinder and let the disk oscillate. When the oscillation ceases, stop the recording and remove the cylinder. To determine the torsional spring constant, measure the radius of the pulley's groove and compute the torque generated by the cylinder's weight. Utilize Equation (3) to calculate the torsional spring constant.

2.2.3. Disk Rotational Inertia

Remove the disk from the second Rotary Motion Sensor and ascertain its mass and radius. Employ a digital scale for this purpose. Utilize the obtained values to calculate the disk's rotational inertia.

2.2.4. Resonance Curves

Attach the magnet to the second Rotary Motion Sensor at the top of the system and position a 6mm glass sheet between the disk and the magnet. Ensure the accuracy of the glass sheet measurements, as some may be incorrect. Adjust the screw until the magnet contacts the sheet and set the signal generator to `Auto`. Begin recording the resonant frequency graph, which may take one or two minutes to appear. The process concludes when the voltage reaches 3.1V or the graph stops moving. Repeat this procedure for 4`mm` and 3`mm` magnet-to-disk distances, maintaining patience as the graph may take some time to display results.

2.2.5. Damping Coefficient

Rather than using the mechanical driver, manually rotate the disk 360 degrees and hold it in position. Press the record button before releasing the disk and stop the recording once the graph ceases to move. Fit a damped sine curve to the graph for further data analysis, recording the coefficients, and comparing them to the theoretical values to determine the damping coefficient (`b`). This approach was also employed in the previous experiment, where the damping distance was set to 3mm, and the mechanical driver was not utilized.

3. Raw Data

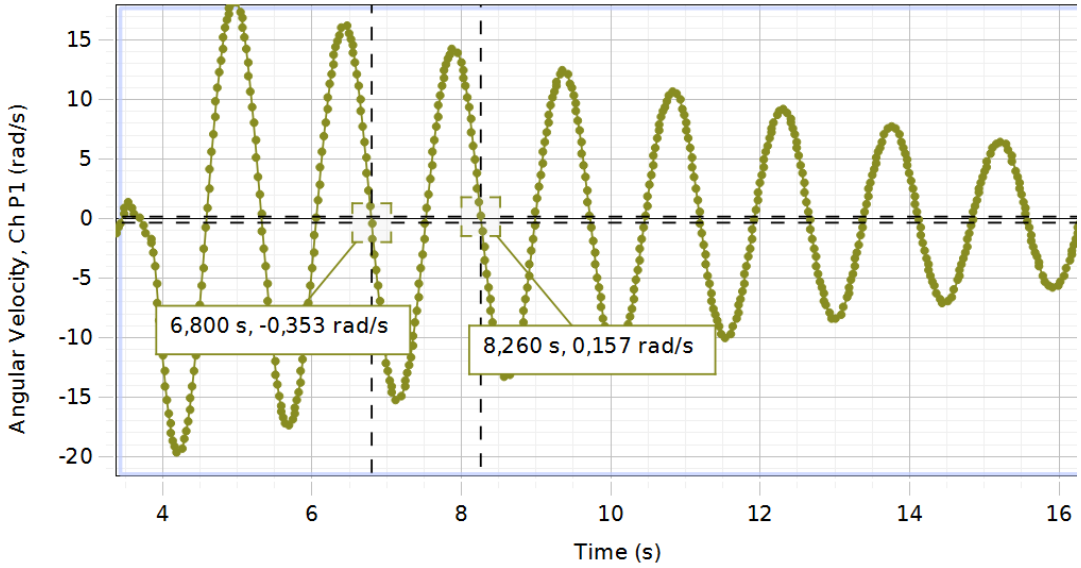

Figure 4: Resonant Frequency Graph

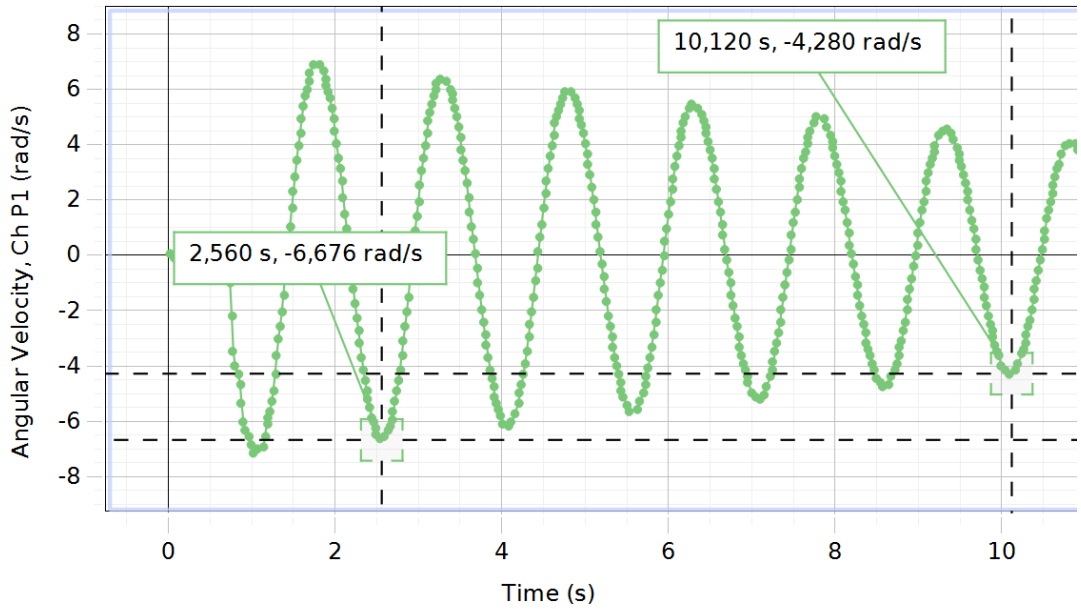

Figure 5: Spring Constant Graph

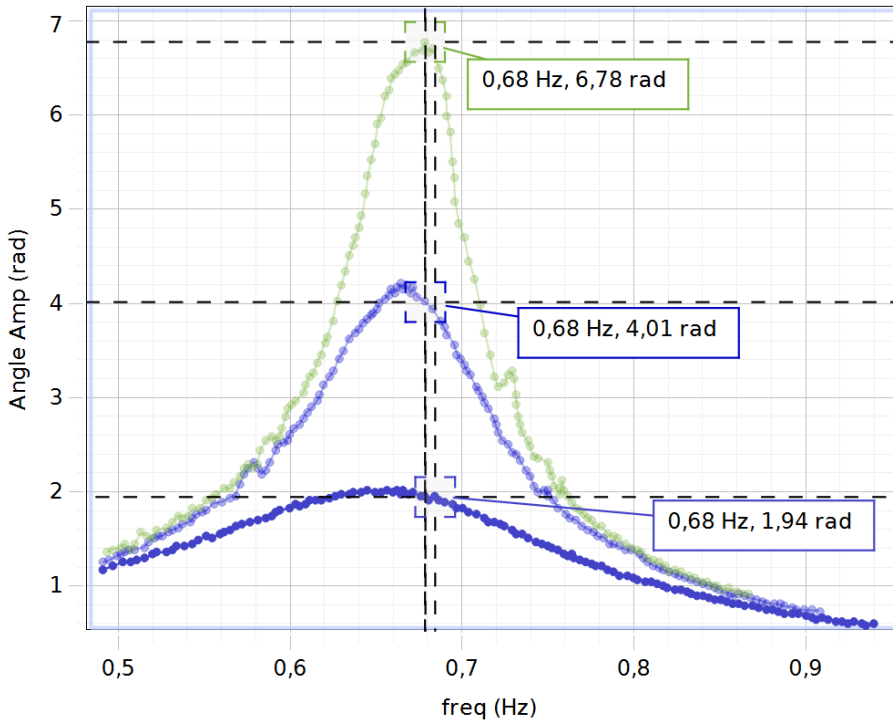

Figure 6: Resonance Frequencies for 3mm, 4mm, and 6mm Thickness

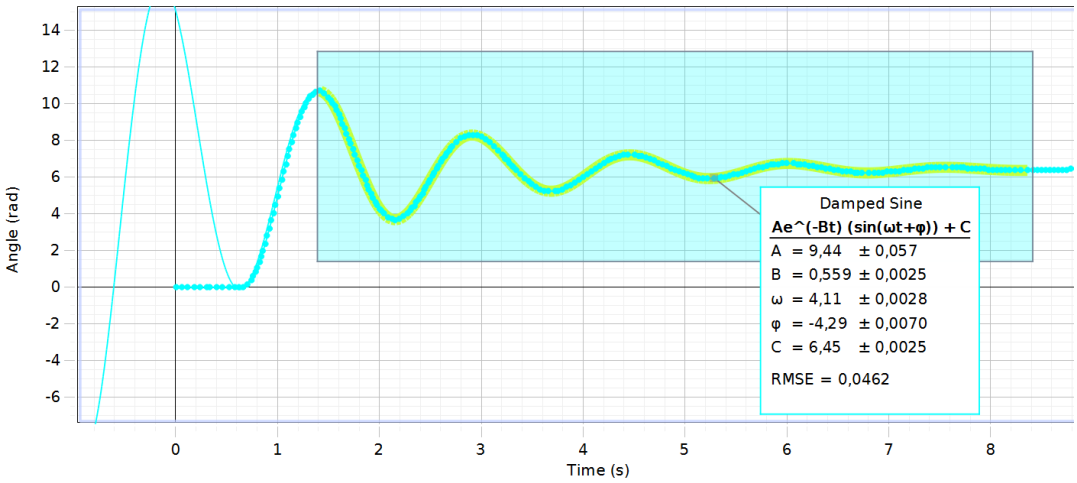

Figure 7: Damping Coefficient 360 degrees

Item	**Mass (g)**	**Radius (m)**
Disk	121.21 ± 0.01	0.047 ± 0.001
Pulley	-	0.096 ± 0.001

Table 1: Mass and Diameter Measurements

4. Data and Error Analysis

4.1. Measurements Error Analysis

An equation

$$\sigma_x = \sqrt{\sum_{i=1}^{n} (\frac{\partial f}{\partial p_i})^2 \sigma_{p_i}^2} \tag{13}$$

can be used to compute the propagation error. Some error measurements are obtained and represented in the following table:

	Uncertainty
Pulley	$\pm 0.01\mathtt{g}$
Rotary Motion Sensor	$\pm 0.00157\mathtt{rad}$
Ruler	$\pm 0.001\mathtt{m}$

4.2. Data Analysis

4.2.1. Resonance Frequency

By using $f = \frac{1}{T}$, we may also obtain the propagation error of $f = \frac{1}{1.460} = 0.685\mathtt{Hz}$ as $\sigma_f = \sqrt{(-\frac{1}{T^2})^2 \sigma_T^2} = (\frac{1}{T})^2 \sigma_T = 0.009\mathtt{Hz}$.

Notice that the value for f here are almost the same with the ones in Figure 6 in which all the three graphs show around $0.68 \pm 0.01\mathtt{Hz}$.

4.2.2. Spring Constant

By substituting both $r = 0.047\mathtt{m}$ and $F = 20g \times 10^{-3}\mathtt{N}$ to $\tau = rF$, we have $\tau = 9.2 \times 10^{-3}\mathtt{Nm}$.

By using equation (3) and (13), we obtain the propagation error κ as

$$\sigma_\kappa = \sqrt{\sum_{i=1}^{n} (\frac{\partial \kappa}{\partial p_i})^2 \sigma_{p_i}^2} = \sqrt{(\frac{\partial \kappa}{\partial \tau})^2 \sigma_\tau^2 + (\frac{\partial \kappa}{\partial \theta})^2 \sigma_\theta^2} = \sqrt{(\frac{1}{\theta})^2 \sigma_\tau^2 + (-\frac{\tau}{\theta^2})^2 \sigma_\theta^2} \tag{14}$$

With both equation (3) and (14), we obtain the torsional spring constant as $\kappa = 2.27 \times 10^{-}3 \pm 0.02 \times 10^{-3} \frac{\mathtt{Nm}}{\mathtt{rad}}$

4.2.3. Disk Rotational Inertia

From equation (2) and (13), we obtain the propagation of error I as

$$\sigma_I = \sqrt{\sum_{i=1}^{n} (\frac{\partial I}{\partial p_i})^2 \sigma_{p_i}^2} = \sqrt{(\frac{\partial I}{\partial M})^2 \sigma_M^2 + (\frac{\partial I}{\partial R})^2 \sigma_R^2} = \sqrt{(\frac{R^2}{2})^2 \sigma_M^2 + (MR)^2 \sigma_R^2} \tag{15}$$

With both equation (2) and (15), we obtain the rotational inertia of the disk and its propagation error. The calculation show that $I = 1.34 \times 10^{-4} \pm 6 \times 10^{-6} \mathtt{kg\ m}^2$

4.2.4. Resonance Curves

Elevating the damping factor influences the curve's configuration by modifying its form. As demonstrated in Figure 6, a broader damping layer results in a diminished maximum amplitude, while the peak frequency remains unaltered. Concurrently, the theoretical frequency is strikingly akin to the genuine resonant frequency, as the discrepancy between them is virtually negligible, rendering the distinction essentially nonexistent. However, the absolute percentage variance is contained within less than 1%. The resonance curve exhibits asymmetry surrounding the resonant frequency, as indicated in equation (9), due to alterations in the dependent variables.

4.2.5. Damping Coefficient

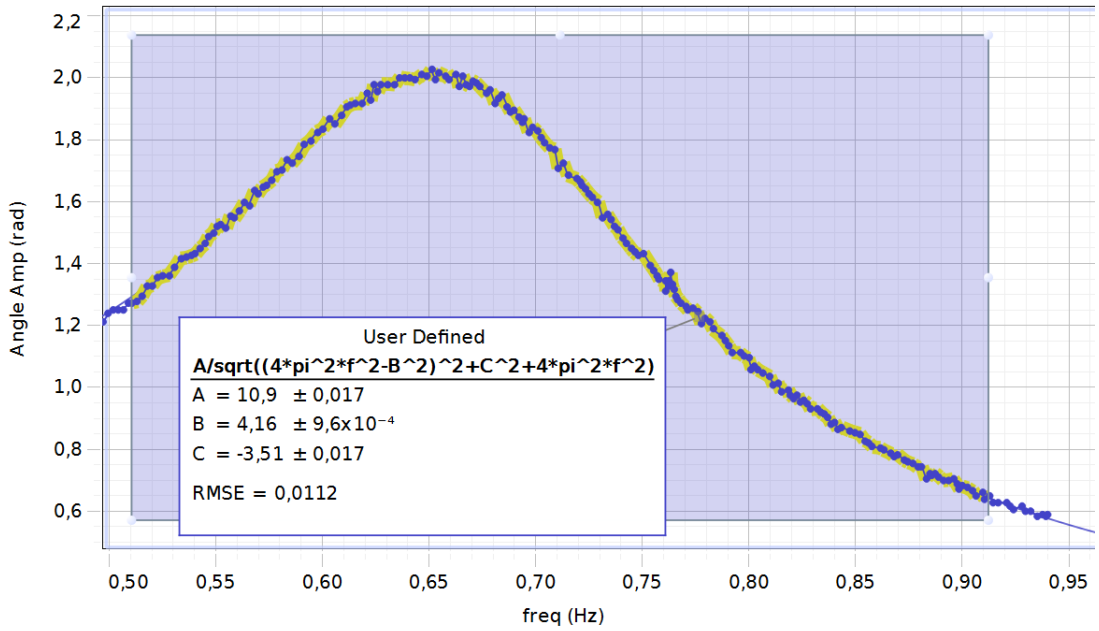

Figure 8: User Defined Fit Resonance Curve

As shown in Figure 8, we obtain $\omega_0 = \mathtt{B} = 4.16$. By using $f = \frac{\omega_0}{2\pi}$, we have $f = 0.662\mathtt{Hz}$. We may obtain the damping constant b by using $b = CI = 1.67 \frac{\mathtt{Ns}}{\mathtt{m}}$.

4.2.6. Phase Analysis

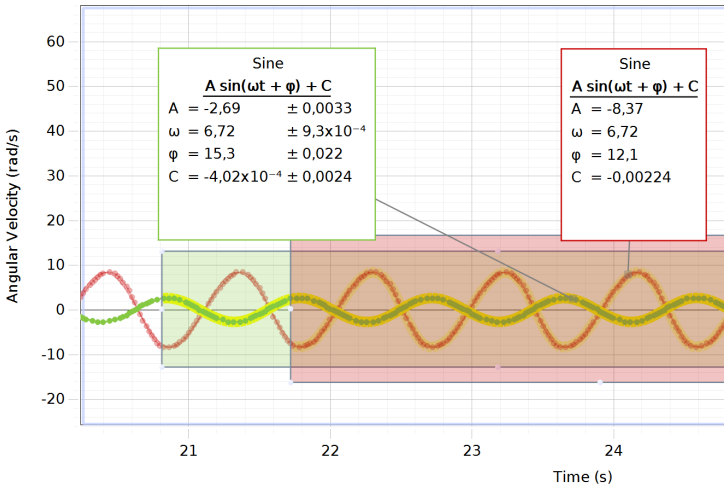

Figure 9: Resonance Curve by 6mm Distance

From Figure 9, we can calculate the phase difference for resonance curve that has 6mm distance of magnet as disk as $\triangle\phi = |\phi_2 - \phi_1| = 3.2 \pm 0.022$ `rad`.

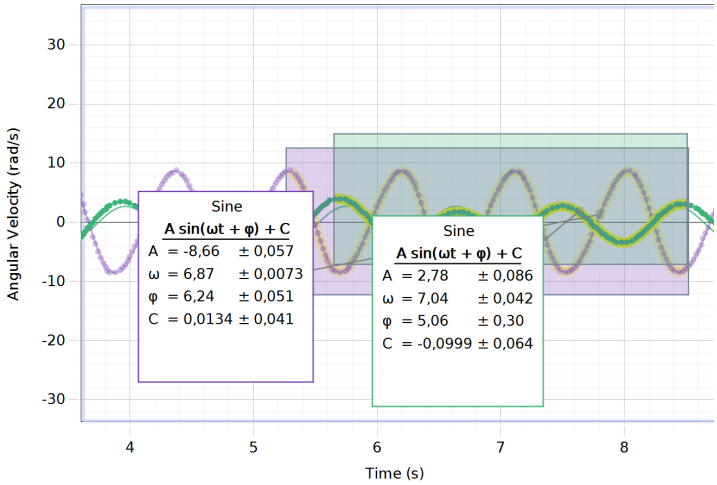

Figure 10: Resonance Curve by 4mm Distance

From Figure 10, we can calculate the phase difference for resonance curve that has 4mm distance of magnet as disk as $\triangle\phi = |\phi_2 - \phi_1| = 1.18 \pm 0.351$ `rad`.

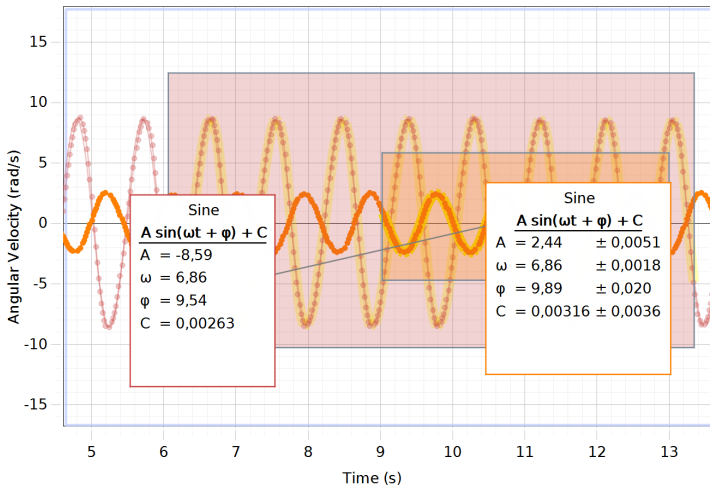

Figure 11: Resonance Curve by 3mm Distance

From Figure 11, we can calculate the phase difference for resonance curve that has 3mm distance of magnet as disk as $\triangle\phi = |\phi_2 - \phi_1| = 0.45 \pm 0.020$ `rad`.

Although each of the figures, respectively, differ from the theoretical value. However, it can be noticed that the value themselves do not differ that much from π, $\frac{\pi}{2}$, and 0, respectively.

5. Limitations

In the course of conducting the experiment, several factors contributed to potential inaccuracies and inconsistencies in the results. Firstly, the precision of the tools utilized for measuring the mass and length of the items was compromised, leading to imprecise measurements. Secondly, the assembly setup, particularly the string connections, was quite unstable, and even the slightest angular deviation could result in a significant difference in force.

Furthermore, the inertial calculations were idealized, as factors such as friction and air resistance were not considered in the analysis. Additionally, the reliability of the software employed for measuring the experiment was questionable, as multiple attempts were required to record the data, casting doubt on the accuracy of the obtained results. Lastly, the springs utilized in the experiment were susceptible to deformation over time, which could render calculations derived from a single measurement inaccurate.

6. Conclusions

In summary, the observed relationship between phase difference and driving frequency aligns with the equation for an externally driven damped harmonic oscillator. The evidence gathered during this investigation supports the notion that the observed phase difference dependence on driving frequency adheres to the presented theoretical models, considering experimental uncertainties.

Research on driven-damped harmonic oscillations has revealed the behavior of physical systems under the influence of external driving forces and damping effects. Utilizing a

spring-mass system subjected to driving and damping forces, the experiment measured alterations in angular velocity and angle. Notable discrepancies emerged upon comparing the theoretical and experimental data for compatibility. Additionally, the investigation examined the asymmetry of resonance curves generated by various dampers, validating the first three Objective section concepts. Nonetheless, the disparities between theoretical and actual results could be attributed to factors such as environmental conditions or human error. Overall, the experiment substantiated the characteristics of driven damped harmonic oscillations.